

Synthesis and Electron Transfer Characteristics of a Neutral, Low-Band-Gap, Mixed-Valence Polyradical

Dörte Reitzenstein,[†] Tatjana Quast,[‡] Florian Kanal,[‡] Martin Kullmann,[‡] Stefan Ruetzel,[‡] Maria S. Hammer,[§] Carsten Deibel,[§] Vladimir Dyakonov,^{§,⊥,¶} Tobias Brixner,^{‡,¶} and Christoph Lambert^{*,†,¶}

[†]Institut für Organische Chemie, [‡]Institut für Physikalische und Theoretische Chemie, and [§]Lehrstuhl für Experimentalphysik VI, Universität Würzburg, Am Hubland, 97074 Würzburg, Germany, [⊥]Functional Materials for Energy Technology, Bavarian Center for Applied Energy Research (ZAE Bayern), Am Hubland, 97074 Würzburg, Germany, and [¶]Wilhelm-Conrad-Röntgen Research Center for Complex Material Systems (RCCM), Würzburg, Germany

Received September 15, 2010. Revised Manuscript Received October 28, 2010

A polyradical consisting of alternating triarylamine and perchlorotriphenylmethyl radical moieties was synthesized by Horner–Emmons reaction. This compound is the first polymeric neutral mixed-valence compound that shows an intervalence charge transfer (IV-CT) band in the NIR. Comparison of the absorption spectra of the polymer with those of a reference monomer shows that the IV-CT transition is confined to one repeating unit. HOMO and LUMO levels are at -5.5 and -4.5 eV vs vacuum, respectively, as estimated by cyclic voltammetry. A very low exciton binding energy is indicated by comparison with the optical band gap (1.2 eV). The electron transfer properties of the polymer were investigated in solution by fs-pump–probe transient absorption spectroscopy. After optical excitation, the polymer shows a biexponential decay in the ps time regime. The short-living, solvent-dependent component refers to the direct decay from the IV-CT state to the ground state and the long-living, solvent-independent component is tentatively attributed to an equilibrium formation of the IV-CT state and a completely charge separated state. The charge-transport properties were investigated in films in organic field-effect transistor (OFET) devices. Electron and hole mobilities are both about $3 \times 10^{-5} \text{ cm}^2 \text{ V}^{-1} \text{ s}^{-1}$, demonstrating ambipolar transport behavior of the polymer.

Introduction

Organic mixed-valence (MV) compounds are widely used as model systems to investigate basic electron transfer (ET) aspects.^{1–4} MV systems usually consist of two or more redox centers with different oxidation states that are connected by conjugated or nonconjugated bridges. ET may then proceed between the redox centers via the bridge thermally or optically induced (Chart 1). The latter is associated with a so-called intervalence charge transfer (IV-CT) absorption band which is usually found in the NIR. This broad absorption band makes MV compounds ideal NIR absorber. Among the various aspects that have been investigated are the distance dependence of ET, the influence of local bridge states (electron-rich vs electron-deficient),^{5,6} the

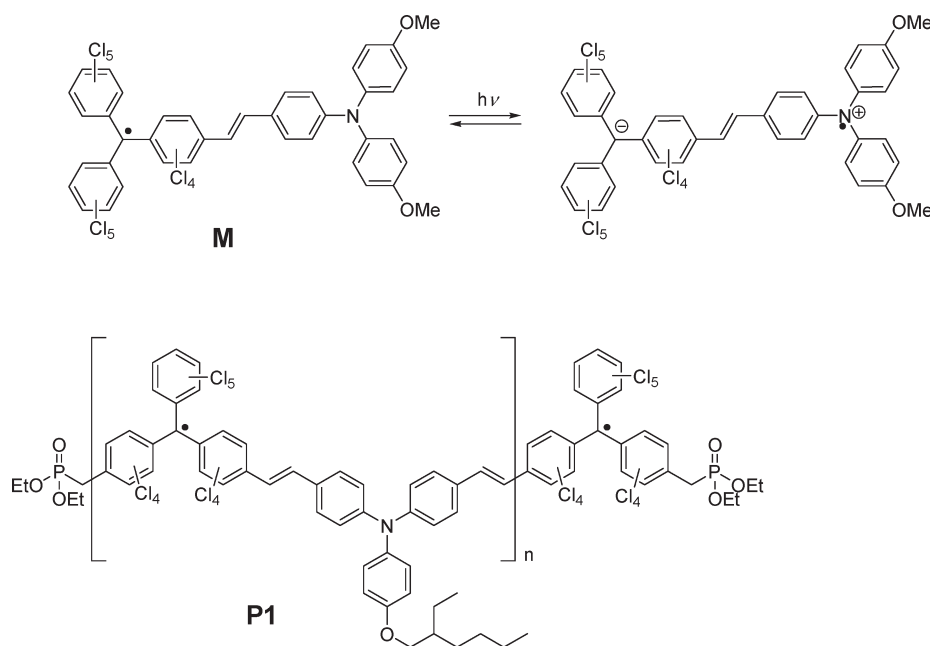
type of the redox centers (e.g., triarylamine,^{7–10} perchlorotriphenylmethyl radicals,^{11–13} hydrazines,^{14,15} dimethoxybenzenes,^{16,17} quinones^{18,19} etc.), temperature,^{20,21} solvent^{22,23} and counterion influences,²⁴ etc. Despite the enormous

*Corresponding author. Phone: +49-(0)931-318-5318. Fax: +49-(0)931-318-7218. E-mail: lambert@chemie.uni-wuerzburg.de.

(1) Brunshwig, B. S.; Creutz, C.; Sutin, N. *Chem. Soc. Rev.* **2002**, *31*, 168–184.
(2) Launay, J.-P. *Chem. Soc. Rev.* **2001**, *30*, 386–397.
(3) Chen, P.; Meyer, T. J. *Chem. Rev.* **1998**, *98*, 1439–1478.
(4) Nelsen, S. F.; Ismagilov, R. F.; Trieber, D. A. *Science* **1997**, *278*, 846–849.
(5) Lambert, C.; Amthor, S.; Schelter, J. J. *Phys. Chem. A* **2004**, *108*, 6474–6486.
(6) Lambert, C.; Nöll, G.; Schelter, J. *Nat. Mater.* **2002**, *1*, 69–73.
(7) Amthor, S.; Lambert, C. J. *Phys. Chem. A* **2006**, *110*, 1177–1189.
(8) Lambert, C.; Nöll, G. J. *Am. Chem. Soc.* **1999**, *121*, 8434–8442.
(9) Lambert, C.; Nöll, G.; Hampel, F. J. *Phys. Chem. A* **2001**, *105*, 7751–7758.

(10) Lambert, C.; Risko, C.; Coropceanu, V.; Schelter, J.; Amthor, S.; Gruhn, N. E.; Durivage, J. C.; Brédas, J.-L. *J. Am. Chem. Soc.* **2005**, *127*, 8508–8516.
(11) Lloveras, V.; Vidal-Gancedo, J.; Ruiz-Molina, D.; Figueira-Duarte, T. M.; Nierengarten, J.-F.; Veciana, J.; Rovira, C. *Faraday Discuss.* **2006**, *131*, 291–305.
(12) Rovira, C.; Ruiz-Molina, D.; Elsner, O.; Vidal-Gancedo, J.; Bonvoisin, J.; Launay, J.-P.; Veciana, J. *Chem.—Eur. J.* **2001**, *7*, 240–250.
(13) Sedó, J.; Ruiz, D.; Vidal-Gancedo, J.; Rovira, C.; Bonvoisin, J.; Launay, J.-P.; Veciana, J. *Adv. Mater.* **1996**, *8*, 748–752.
(14) Nelsen, S. F.; Konradsson, A. E.; Teki, Y. J. *Am. Chem. Soc.* **2006**, *128*, 2902–2910.
(15) Nelsen, S. F.; Ismagilov, R. F.; Powell, D. R. *J. Am. Chem. Soc.* **1997**, *119*, 10213–10222.
(16) Lindeman, S. V.; Rosokha, S. V.; Sun, D.; Kochi, J. K. *J. Am. Chem. Soc.* **2002**, *124*, 843–855.
(17) Sun, D.-L.; Rosokha, S. V.; Lindeman, S. V.; Kochi, J. K. *J. Am. Chem. Soc.* **2003**, *125*, 15950–15963.
(18) Rak, S. F.; Miller, L. L. *J. Am. Chem. Soc.* **1992**, *114*, 1388–1394.
(19) Jozefiak, T. H.; Almlof, J. E.; Feyereisen, M. W.; Miller, L. L. *J. Am. Chem. Soc.* **1989**, *111*, 4105–4106.
(20) Coropceanu, V.; Lambert, C.; Nöll, G.; Brédas, J.-L. *Chem. Phys. Lett.* **2003**, *373*, 153–160.
(21) Nelsen, S. F.; Ismagilov, R. F.; Gentile, K. E.; Powell, D. R. *J. Am. Chem. Soc.* **1999**, *121*, 7108–7114.
(22) Nelsen, S. F.; Trieber, D. A.; Ismagilov, R. F.; Teki, Y. J. *Am. Chem. Soc.* **2001**, *123*, 5684–5694.
(23) Nelsen, S. F.; Tran, H. Q. *J. Phys. Chem. A* **1999**, *103*, 8139–8144.
(24) Nelsen, S. F.; Ismagilov, R. F. *J. Phys. Chem. A* **1999**, *103*, 5373–5378.

Chart 1



amount of data collected on the many different MV compounds and the wealth of knowledge that has been gained by their interpretation, MV compounds have only rarely been used as optoelectronic materials.²⁵ Although polymeric MV compounds are known,^{25–27} the major reason for the lack of practical application is the fact that almost all MV compounds are radical ions that are generated in situ and are insoluble in nonpolar solvents. This hampers their processing and their practical use as, for example, electron- or hole-conducting materials or NIR absorber. The solubility issue has recently been overcome by the design of neutral open-shell MV compounds that consist of a triarylamine donor and a perchlorotriphenylmethyl (PCTM) radical acceptor, for example, compound **M** (Chart 1).^{28–30} These systems are soluble in a broad variety of solvents ranging from apolar cyclohexane to strongly polar acetonitrile. However, their film-forming properties are still insufficient for practical use. Thus, the aim of this work is to synthesize and investigate the first neutral MV polymer **P1** that consists of alternating triarylamine and PCTM redox centers along the polymer backbone (Chart 1).

Triarylamines are widely used as hole conductors in optoelectronic devices such as photocopier machines,

OLEDs, and solar cells.^{31–33} Triarylamines combine the advantage of easy synthetic accessibility and low reorganization energy,^{34,35} (see below) which promotes fast ET. PCTM radicals, on the other hand, are excellent electron acceptors that have been incorporated in polymers,³⁶ used as the spin bearing unit in organic magnets,^{37–39} and attached to surfaces, etc.^{40–43} However, before we discuss the polymer aspects, we will briefly outline the concept of mixed valency in context with ET phenomena.

In Figure 1, the adiabatic potential energy surfaces (PES) of the ground and the excited state of a MV system with two nondegenerate redox centers (= two redox states) together with the harmonic potentials of the two diabatic (formally noninteracting) states along an ET coordinate x are displayed. The two diabatic states are coupled by the electronic coupling matrix element V_{12} ,

- (25) Nishikitani, Y.; Kobayashi, M.; Uchida, S.; Kubo, T. *Electrochim. Acta* **2001**, *46*, 2035–2040.
 (26) Chou, M.-Y.; Leung, M.-K.; Su, Y. O.; Chiang, C. L.; Lin, C.-C.; Liu, J.-H.; Kuo, C.-K.; Mou, C.-Y. *Chem. Mater.* **2004**, *16*, 654–661.
 (27) Lambert, C.; Nöll, G. *Synth. Met.* **2003**, *139*, 57–62.
 (28) Heckmann, A.; Dümmler, S.; Pauli, J.; Margraf, M.; Köhler, J.; Stich, D.; Lambert, C.; Fischer, I.; Resch-Genger, U. *J. Phys. Chem. C* **2009**, *113*, 20958–20966.
 (29) Heckmann, A.; Lambert, C. *J. Am. Chem. Soc.* **2007**, *129*, 5515–5527.
 (30) Heckmann, A.; Lambert, C.; Goebel, M.; Wortmann, R. *Angew. Chem., Int. Ed.* **2004**, *43*, 5851–5856.
 (31) Shirota, Y.; Kageyama, H. *Chem. Rev.* **2007**, *107*, 953–1010.
 (32) Thelakkat, M. *Macromol. Mater. Eng.* **2002**, *287*, 442–461.

- (33) Weiss, D. S.; Cowdery, J. R.; Young, R. H. *Electron Transfer in Chemistry*; Balzani, V., Ed.; Wiley-VCH: Weinheim, Germany, 2001; Vol. 5.
 (34) Lin, B. C.; Cheng, C. P.; Lao, Z. P. M. *J. Phys. Chem. A* **2003**, *107*, 5241–5251.
 (35) Malagoli, M.; Brédas, J. L. *Chem. Phys. Lett.* **2000**, *327*, 13–17.
 (36) Domingo, V. M.; Castañer, J.; Riera, J.; Fajará, L.; Labarta, A. *Chem. Mater.* **1995**, *7*, 314–323.
 (37) MasPOCH, D.; Domingo, N.; Ruiz-Molina, D.; Wurst, K.; Tejada, J.; Rovira, C.; Veciana, J. *J. Am. Chem. Soc.* **2004**, *126*, 730–731.
 (38) MasPOCH, D.; Domingo, N.; Ruiz-Molina, D.; Wurst, K.; Vaughan, G.; Tejada, J.; Rovira, C.; Veciana, J. *Angew. Chem., Int. Ed.* **2004**, *43*, 1828–1832.
 (39) MasPOCH, D.; Ruiz-Molina, D.; Wurst, K.; Domingo, N.; Cavallini, M.; Biscarini, F.; Tejada, J.; Rovira, C.; Veciana, J. *Nat. Mater.* **2003**, *2*, 190–195.
 (40) Crivillers, N.; Mas-Torrent, M.; Perruchas, S.; Roques, N.; Vidal-Gancedo, J.; Veciana, J.; Rovira, C.; Basabe-Desmonts, L.; Ravoo, B. J.; Crego-Calama, M.; Reinhoudt, D. N. *Angew. Chem., Int. Ed.* **2007**, *46*, 2215–2219.
 (41) Crivillers, N.; Mas-Torrent, M.; Vidal-Gancedo, J.; Veciana, J.; Rovira, C. *J. Am. Chem. Soc.* **2008**, *130*, 5499–5506.
 (42) Crivillers, N.; Munuera, C.; Mas-Torrent, M.; Simão, C.; Bromley, S. T.; Ocal, C.; Rovira, C.; Veciana, J. *Adv. Mater.* **2009**, *21*, 1177–1181.
 (43) Mas-Torrent, M.; Crivillers, N.; Mugnaini, V.; Ratera, I.; Rovira, C.; Veciana, J. *J. Mater. Chem.* **2009**, *19*, 1691–1695.

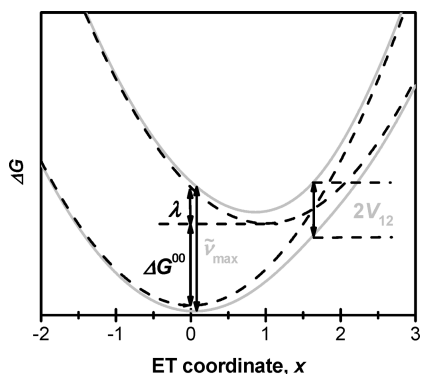


Figure 1. Diabatic (dashed black) and adiabatic (solid gray) potential energy surfaces (PES) of a one-dimensional MV system with two non-degenerate redox centers. V_{12} = coupling integral, λ = Marcus reorganization energy, ΔG^{00} = difference of the free energy between the diabatic states.

which is a measure for the interaction between the two diabatic redox states (electron mainly located at the one or the other redox center). An ET process can be optically induced from the adiabatic ground state to the excited state by excitation into the IV-CT band. In context of the generalized Mulliken–Hush theory (GMH)^{44–47} the parameters describing the ET can be evaluated by analyzing the IV-CT band.^{48–50} In the weak coupling regime where V_{12} vanishes, the maximum of the IV-CT band $\tilde{\nu}_{\max}$ corresponds to the sum of the Marcus reorganization energy λ and the difference of the free energies of the minima of the diabatic states ΔG^{00} (Figure 1). The reorganization energy λ can be divided into two terms: the outer solvent reorganization energy, λ_o , which characterizes the energy needed for the reorientation of the solvent molecules after the ET event and the inner vibrational reorganization energy, λ_v , which is associated with geometrical changes of the molecule during ET. In the present case, V_{12} is so strong (ca. 2000 cm^{-1} as estimated from monomer **M**)²⁹ compared to the reorganization energy that no double minimum potential is present in the ground state adiabatic potential curve.

In recent studies, we were able to separate the various ET parameters for a series of neutral MV compounds similar to **M** by applying Bixon–Jortner theory to the IV-CT band analysis.^{28,29} This analysis explains the lack of almost any solvatochromism of the IV-CT band for this class of MV species by the compensating trends of ΔG^{00} and λ with solvent polarity. Further analysis of these parameters as well as electrooptical absorption measurements yield a difference of dipole moments in the ground and excited state of ca. 19 D ,⁵¹ which emphasizes the CT character of **M**. Transient absorption spectra prove the

optically induced ET by assigning transient signals as being due to localized excitations of triarylamine radical cation and PCTM anion moieties.^{28,52,53}

In this publication, we focus on some optical and ET issues of the first neutral MV polyradical **P1**, which was synthesized by Horner–Emmons reaction to yield a soluble polymer of $\bar{M}_w = 19300\text{ Da}$ ($\bar{M}_n = 11200\text{ Da}$, PDI = 1.72). In the following, its synthesis and steady state absorption properties as well as results of cyclic voltammetry, spectroelectrochemistry, fs-pump–probe transient absorption spectroscopy, and preliminary characteristics of an OFET device will be presented.

Experimental Section

Materials. CuBr_2 and K_2CO_3 were dried under vacuum above $200\text{ }^\circ\text{C}$ and stored under a nitrogen atmosphere. 18-crown-6 was distilled under reduced pressure and stored under nitrogen atmosphere. Cu powder was activated by the following procedure:⁵⁴ Cu powder (2.00 g) was stirred in acetone (20 mL) with I_2 (40.0 mg) for 10 min, filtered, and subsequently stirred in conc. HCl/acetone 1:1 (20 mL) for 5 min. The activated Cu powder was filtered, washed thoroughly with acetone until neutral and dried under a vacuum. All other chemicals and reagents were used as received. For reactions carried out under a nitrogen atmosphere, standard Schlenk techniques were used.

Characterization. NMR spectra were recorded with either a Bruker AVANCE 400 FT-NMR spectrometer or a Bruker AVANCE DMX 600 FT-NMR spectrometer at r.t.. Chemical shifts δ are given in ppm vs tetramethylsilane. Carbon atoms connected to chlorine (CCl) were distinguished from those surrounded by only carbon (quart.) by the observation of a shoulder peak with one-third of the main peak's intensity according to the isotopic distribution of ^{35}Cl and ^{37}Cl . Mass spectra were recorded with a Finnigan MAT 90 or with a Bruker Daltonics micrOTOF focus mass spectrometer equipped with an APCI ion source (Agilent G1947–60101). For calculations of the respective mass values of the isotopic distribution, the software modul “Bruker Daltonics IsotopePattern” of the software Compass 1.1 from Bruker Daltonik GmbH, Bremen was used. Due to the isotopic distribution over a broad m/z region caused by chlorine the monoisotopic signal was too small in intensity for some compounds for an accurate mass measurement. In this case, typically the most intense signal ($X+n$) of this isotopic distribution was taken as described and compared with the respective calculated value. GPC measurements were performed with a setup consisting of a dual-plunger, tandem-flow pump (Shimadzu, LC-10AT), a He-degasser unit (Shimadzu, DGU-10B), two SDV columns (PSS, Mainz, Germany; pore size, 100 and $1 \times 10^3\text{ \AA}$; particle size, $5\text{ }\mu\text{m}$; column length, 300 mm each) and a Gynkotec model 160 UV detector. The eluent was THF (Acros, HPLC grade) at $35\text{ }^\circ\text{C}$ with a flow rate of 1 mL min^{-1} . The calibration curve was made with a series of monodisperse polystyrene standards (PSS, Mainz, Germany; concentration: 1 mg/mL). IR spectra were recorded on a JASCO FT/IR 4100 instrument using KBr pellets. DSC measurements were performed on a Mettler-Toledo DSC 823 under a nitrogen atmosphere.

(44) Cave, R. J.; Newton, M. D. *Chem. Phys. Lett.* **1996**, *249*, 15–19.
 (45) Cave, R. J.; Newton, M. D. *J. Chem. Phys.* **1997**, *106*, 9213–9226.
 (46) Creutz, C.; Newton, M. D.; Sutin, N. *J. Photochem. Photobiol. A: Chem.* **1994**, *82*, 47–59.
 (47) Newton, M. D. *Adv. Chem. Phys.* **1999**, *106*, 303–375.
 (48) Hush, N. S. *Mixed-Valence Compounds*; Brown, D. B., Ed.; D. Reidel Publishing Company: Dordrecht, The Netherlands, 1980.
 (49) Hush, N. S. *Coord. Chem. Rev.* **1985**, *64*, 135–157.
 (50) Reimers, J. R.; Hush, N. S. *Chem. Phys.* **1989**, *134*, 323–354.
 (51) Heckmann, A.; Lambert, C.; Goebel, M.; Wortmann, R. *Angew. Chem., Int. Ed.* **2004**, *43*, 5851–5856.

(52) Duemmler, S.; Roth, W.; Fischer, I.; Heckmann, A.; Lambert, C. *Chem. Phys. Lett.* **2005**, *408*, 264–268.
 (53) Maksimenka, R.; Margraf, M.; Köhler, J.; Heckmann, A.; Lambert, C.; Fischer, I. *Chem. Phys.* **2008**, *347*, 436–445.
 (54) McKeown, N. B.; Badriya, S.; Helliwell, M.; Shkunov, M. *J. Mater. Chem.* **2007**, *17*, 2088–2094.

Bis(2,3,4,5,6-pentachlorophenyl)-2,3,5,6-tetrachloro-4-((1E),2-[4-(bis(4-methoxyphenyl)amino)-phenyl]ethenyl)phenylmethyl radical M.³⁰ To a solution of the α -H compound³⁰ of **M** (55.6 mg, 52.6 μ mol) in dry THF (5 mL) was added *n*-Bu₄NOH (70.1 μ L, 105 μ mol, \sim 1.5 M in H₂O) under the exclusion of air and light, and the deep blue solution was stirred for 1 h during which it turned deep purple. After the addition of *p*-chloranil (33.2 mg, 135 μ mol), the resulting brown solution was stirred for 16 h. The solvent was removed and the mixture was diluted in dichloromethane and washed twice with slightly acidic water (\sim 0.01 N), four times with sodium hydroxide solution (5%), and twice with water. The organic phase was dried over MgSO₄, the solvent was removed, and the raw product was purified by flash chromatography (petrol ether/dichloromethane 1:1). Further purification by repeated dropwise addition of a concentrated acetone solution into methanol gave a brown solid. Yield: 31.8 mg (30.1 μ mol, 57%).

4,4'-Dimethyltriphenylmethane 1.⁵⁵ To a solution of 4-methylphenylmagnesium bromide (40.6 g, 237 mmol) in 180 mL diethylether a solution of *p*-methylbenzophenone (28.1 g, 143 mmol) in 150 mL diethylether was added dropwise over a period of 1 h. Subsequently, the red reaction mixture was refluxed for 1 h, poured onto crushed ice and acidified with 6 N HCl (pH 3–4). The phases were separated and the aqueous phase was extracted with diethylether (3 \times 100 mL). The combined organic extracts were washed with water (3 \times 100 mL) and dried over MgSO₄. After removal of the solvent formic acid (175 mL, 98–100%) was added and the dark green mixture was refluxed for 3 h, whereupon it turned brown. Then it was poured onto crushed ice and after addition of diethylether the aqueous phase was separated and extracted with diethylether (3 \times 75 mL). The combined organic phases were washed with saturated NaHCO₃ until neutral and dried over MgSO₄. Evaporation of the solvent and purification by flash chromatography (petrol ether/dichloromethane 10:1) gave an oily product, which could be crystallized from *n*-hexane at -30 °C. Yield: 22.8 g (83.7 mmol, 59%) of colorless needles. ¹H NMR (400 MHz, CDCl₃): δ = 7.30–7.24 (m, 2H, phenyl), 7.22–7.17 (m, 1H, phenyl), 7.13–7.10 (m, 2H, phenyl), 7.09 (AA', 4H, phenyl), 7.00 (BB', 4H, phenyl), 5.48 (s, 1H, CH), 2.32 (s, 6H, CH₃).

[Bis(4-methyl-2,3,5,6-tetrachlorophenyl)-(2,3,4,5,6-pentachlorophenyl)methane 2. To a hot solution (70 °C) of S₂Cl₂ (3.42 g, 25.3 mmol) and anhydrous AlCl₃ (1.73 g, 13.0 mmol) in SO₂Cl₂ (400 mL) a solution of **1** (9.07 g, 33.3 mmol) in SO₂Cl₂ (200 mL) was added dropwise over the course of 1 h. After 8 h of heating, during which the reaction volume was kept constant by addition of further SO₂Cl₂, the latter was removed by distillation first at atmospheric pressure and then in vacuum. Water (500 mL) was added and the mixture was made basic by the addition of NaHCO₃, whereupon it was heated to reflux during 1 h. The cooled mixture was acidified with conc. HCl (ca. 50 mL) and the solid was filtered off and washed with water. The crude product was repeatedly heated to reflux in *n*-hexane and filtered off until the *n*-hexane filtrate remained colorless. Yield: 15.0 g (20.8 mmol, 63%) of a gray solid. Decomposition: 313 °C (*n*-hexane). ¹H NMR (600 MHz, CDCl₃): δ = 6.99 (s, 1H, CH), 2.62 (s, 6H, CH₃). ¹³C NMR (151 MHz, CDCl₃): δ = 137.2 (quart.), 137.11 (quart.), 137.09 (quart.), 135.53 (quart.), 135.49 (quart.), 135.2 (CCI), 134.3 (CCI), 134.224 (CCI), 134.220 (CCI), 134.1 (CCI), 134.0 (CCI), 133.32 (CCI), 133.25 (CCI), 133.24 (CCI), 133.22 (CCI), 133.11 (CCI), 133.05 (CCI), 132.2 (CCI), 56.4 (CH), 20.633 (CH₃), 20.631(CH₃). APCI neg. (high-resolution):

[M–H⁺][–] calcd for C₂₁H₆Cl₁₃[–], 712.64258; found, 712.64225 (Δ = 0.47 ppm).

[Bis(4-bromomethyl-2,3,5,6-tetrachlorophenyl)-(2,3,4,5,6-pentachlorophenyl)methane 3. A mixture of **2** (5.00 g, 6.94 mmol), *N*-bromosuccinimide (12.4 g, 69.4 mmol), azobis(isobutyronitrile) (273 mg, 1.67 mmol), and CCl₄ (150 mL) was refluxed for 60 h. During the reaction, *N*-bromosuccinimide (4 \times 2.48 g, 4 \times 13.9 mmol) and azobis(isobutyronitrile) (4 \times 227 mg, 4 \times 1.39 mmol) were added every 10–14 h. The reaction mixture was cooled to r.t., filtered, washed with CCl₄, and dried in a vacuum. The crude product was refluxed in MeOH/CHCl₃ (5:1 and 1:1), cooled to r.t., filtered off, and dried in a vacuum. Yield: 4.98 g (5.67 mmol, 82%) of a yellowish solid. Decomposition: 218 °C (MeOH/CHCl₃). ¹H NMR (600 MHz, CDCl₃): δ = 7.02 (s, 1H, CH), 4.816 (s, 2H, CH₂), 4.814 (s, 2H, CH₂). ¹³C NMR (151 MHz, CDCl₃): δ = 138.0 (2C, quart.), 136.25 (quart.), 136.21 (quart.), 136.20 (quart.), 135.09 (CCI), 135.07 (CCI), 135.0 (CCI), 134.59 (CCI), 134.58 (CCI), 134.03 (CCI), 134.01 (CCI), 133.96 (CCI), 133.7 (CCI), 133.53 (CCI), 133.47 (CCI), 133.46 (CCI), 132.5 (CCI), 56.7 (CH), 28.9 (2C, CH₂). ESI neg. (high resolution): calcd for X+8 of [M][–] = C₂₁H₅Cl₁₃Br₂[–], 876.45291; found, 876.45248 (Δ = 0.50 ppm).

[Bis(4-diethylphosphonomethyl-2,3,5,6-tetrachlorophenyl)-(2,3,4,5,6-pentachlorophenyl)methane 4. Under a nitrogen atmosphere, a mixture of **3** (3.42 g, 3.90 mmol) in degassed triethyl phosphite (15.6 mL) was heated to 180 °C (2 h). Triethyl phosphite was removed under reduced pressure (155 °C/0.03 mbar at the end of removal). The crude product was purified by flash chromatography (ethyl acetate/acetone 5:1). Yield: 3.54 g (3.57 mmol, 91%) of a colorless solid. M.p.: 89 °C (ethyl acetate/acetone). ¹H NMR (400 MHz, CD₂Cl₂): δ = 7.01 (t, ⁷J_{PH} = 1.9 Hz, 1H, CH), 4.04 (m, 8H, OCH₂CH₃), 3.73 (d, ²J_{PH} = 22.5 Hz, 4H, CH₂), 1.24 (td, ³J_{HH} = 7.1 Hz, ⁴J_{PH} = 1.3 Hz, 12H, OCH₂CH₃). ¹³C NMR (101 MHz, CDCl₃, P decoupled): δ = 136.8 (quart.), 136.66 (quart.), 136.63 (quart.), 135.0 (CCI), 134.78 (CCI), 134.76 (2C, CCI), 134.7 (CCI), 133.9 (CCI), 133.75 (CCI), 133.72 (CCI), 133.68 (CCI), 133.67 (CCI), 133.52 (CCI), 133.47 (CCI), 132.69 (quart.), 132.67 (quart.), 132.4 (CCI), 62.5 (4C, OCH₂CH₃), 56.7 (CH), 33.1 (2C, CH₂), 16.33 (2C, OCH₂CH₃), 16.32 (2C, OCH₂CH₃). ³¹P NMR (162 MHz, CDCl₃): δ = 21.9. ESI pos. (high resolution): calcd for X+6 of [M + NH₄⁺]⁺ = C₂₉H₂₉Cl₁₃NO₆P₂⁺, 1009.73325; found, 1009.73317 (Δ = 0.08 ppm).

Poly{[(bis(2,3,5,6-tetrachlorophenyl)-2,3,4,5,6-pentachlorophenyl)methane-4,4'-diyl]-alt-[4,4'-bis(vinylphenyl)-4-(2-ethylhexyloxy)phenylamine]} 7. Under a nitrogen atmosphere, **4** (475 mg, 479 μ mol) and **6**^{56,57} (200 mg, 466 μ mol) were dissolved in dry THF (4.65 mL). To the yellow solution was added KO^tBu (113 mg, 1.01 mmol) in four portions and the mixture was stirred at r.t. for 3 h. The resulting black, viscous liquid was poured onto 100 mL of 0.01 M HCl to give a yellow precipitate that was stirred for a few minutes, filtered off, and washed with water and acetone. The crude product was washed in a Soxhlet apparatus with acetone overnight, dried, dissolved in THF and precipitated by dropwise addition of the concentrated THF solution into *n*-hexane. Yield: 378 mg (339 μ mol, 73%) of a yellow solid. Decomposition: 293 °C (THF/*n*-hexane). ¹H NMR (600 MHz, [D₈]THF): δ = 7.47 (AA', 4H, phenyl), 7.13 (s, 1H, CH_{PCTM}), 7.12–7.01 (10H, AA', BB' and C–CH=CH–C), 6.92 (BB', 2H, phenyl), 3.88 (d, ³J_{HH} = 5.6 Hz, 2H, OCH₂(ethylhexyl)), 1.72 (s, 1H, CH(ethylhexyl)),⁵⁸ 1.59–1.30 (m, 8H,

(55) Brook, A. G.; Gilman, H.; Miller, L. S. *J. Am. Chem. Soc.* **1953**, *75*, 4759–4765.

(56) Karastatiris, P.; Mikroyannidis, J. A.; Spiliopoulos, I. K. *J. Polym. Sci. A: Polym. Chem.* **2008**, *46*, 2367–2378.

(57) Hua, J.; Meng, F.; Li, J.; Ding, F.; Fan, X.; Tian, H. *Eur. Polym. J.* **2006**, *42*, 2686–2694.

(58) The signal is hidden below the THF signal as confirmed by comparison with the spectrum in CD₂Cl₂.

$\text{CH}_2(\text{ethylhexyl})$), 0.96 ($t, {}^3J_{\text{HH}} = 7.5 \text{ Hz}$, 3H, $\text{CH}_3(\text{ethylhexyl})$), 0.92 ($t, {}^3J_{\text{HH}} = 6.9 \text{ Hz}$, 3H, $\text{CH}_3(\text{ethylhexyl})$). ^{13}C NMR (151 MHz, $[\text{D}_8]\text{THF}$): $\delta = 157.9$ (quart.), 149.4 (2C, quart.), 140.4 (quart.), 139.21 (quart.), 139.18 (quart.), 139.1 (2C, CH), 138.3 (quart.), 136.98 (quart.), 136.95 (quart.), 136.1 (quart.), 135.7 (quart.), 135.6 (quart.), 134.9 (quart.), 134.71 (quart.), 134.68 (quart.), 134.3 (quart.), 134.28 (quart.), 134.2 (quart.), 134.17 (quart.), 133.2 (quart.), 133.11 (quart.), 133.08 (quart.), 130.8 (2C, quart.), 128.8 (4C, CH), 128.6 (2C, CH), 123.5 (4C, CH), 121.7 (2C, CH), 116.3 (2C, CH), 71.1 ($\text{OCH}_2(\text{ethylhexyl})$), 57.8 (CH_{PCTM}), 40.6 ($\text{CH}(\text{ethylhexyl})$), 31.5 ($\text{CH}_2(\text{ethylhexyl})$), 30.0 ($\text{CH}_2(\text{ethylhexyl})$), 24.8 ($\text{CH}_2(\text{ethylhexyl})$), 23.9 ($\text{CH}_2(\text{ethylhexyl})$), 14.4 ($\text{CH}_3(\text{ethylhexyl})$), 11.5 ($\text{CH}_3(\text{ethylhexyl})$). GPC (THF): $M_w = 17100 \text{ Da}$, $M_n = 9600 \text{ Da}$, PDI = 1.77. IR: $\tilde{\nu}/\text{cm}^{-1} = 3037$ (w), 2956 (m), 2927 (m), 2869 (m), 2860 (m), 1628 (w), 1595 (s), 1540 (w), 1506 (s), 1466 (w), 1365 (m), 1316 (s), 1292 (s), 1269 (v), 1240 (s), 1191 (w), 1178 (m), 1164 (w), 1139 (w), 1105 (w), 1028 (w), 967 (w), 910 (w), 809 (m), 728 (w).

Poly{[(bis(2,3,5,6-tetrachlorophenyl)-2,3,4,5,6-pentachlorophenyl)methyl radical-4,4'-diyl]-alt-[4,4'-bis(vinylphenyl)-4-(2-ethylhexyloxy)phenylamine]} **P1**. Under a nitrogen atmosphere, **7** (100 mg, 89.8 μmol) was dissolved in dry THF (4.5 mL). *n*-Bu₄NOH (125 μL , 188 μmol , $\sim 1.5 \text{ M}$ in H₂O) was added, whereupon the color of the reaction mixture immediately changed from yellow to dark blue. After 1 h of stirring at r.t., *p*-chloranil (57.4 mg, 233 μmol) was added and the dark brown mixture was further stirred at r.t. for 21 h before being dropped into a mixture of acetone (70 mL) and 2 N HCl (0.12 mL) to give a dark brown precipitate that was separated by centrifugation and washed with MeOH. The product was dissolved in THF, dropped into acetone/2 N HCl (70 mL/0.12 mL), centrifuged and washed with MeOH two more times. Finally the product was washed with acetone in a Soxhlet apparatus overnight. Yield: 88.6 mg (79.6 μmol , 89%) of a dark brown powder. Decomposition: 250 °C (DSC measurement, acetone). GPC (THF): $M_w = 19300 \text{ Da}$, $M_n = 11200 \text{ Da}$, PDI = 1.72. IR: $\tilde{\nu}/\text{cm}^{-1} = 3033$ (w), 2953 (m), 2924 (m), 2869 (m), 2860 (m), 1592 (s), 1506 (s), 1467 (w), 1426 (w), 1379 (w), 1335 (v), 1323 (s), 1287 (m), 1259 (s), 1239 (s), 1225 (v), 1192 (w), 1178 (s), 1164 (m), 1027 (w), 964 (w), 814 (w), 737 (w), 661 (w).

UV-vis-NIR Spectroscopy. Absorption spectra were recorded on a JASCO V-570 UV/vis/NIR spectrometer in 1 cm quartz cells (Hellma) at r.t.. All solvents were of spectroscopic grade and used as received. For solid state absorption spectra thin films were prepared by spin coating toluene or chlorobenzene solutions (5 mg/mL, 4000 rpm, 60 s) of the polymer onto quartz plates. For the determination of the full-width at half-maximum $\tilde{\nu}_{1/2}$ the IV-CT band was fitted with three (dichloromethane) and four (toluene) Gaussian bands, respectively, and the sum of the two (dichloromethane) and three (toluene) Gaussian bands with the lowest energy was used for the determination of $\tilde{\nu}_{1/2}$.

Electrochemistry. Cyclic voltammetric (CV) experiments were carried out with a BAS CV-50 W instrument (Software Version 2.0). A conventional three-electrode setup consisting of a platinum disk working electrode (2 mm in diameter), an Ag/AgCl pseudoreference electrode and a platinum wire counter electrode was used. The redox potentials were referenced against the ferrocene/ferrocenium (Fc/Fc^+) redox couple as an internal standard. Measurements were performed under an argon atmosphere in dichloromethane with 0.2 M tetrabutylammonium hexafluorophosphate (TBAPF₆) as the supporting electrolyte. Dichloromethane (Baker, HPLC grade) was predried over molecular sieves 4 Å (Acros, 8–12 mesh) and distilled over CaH₂. For thin layer measurements ($20 \pm 5 \mu\text{m}$) the working electrode was placed on the polished plane of a flexible glass

hemisphere ($\text{Ø} = 8 \text{ mm}$). Differential pulse voltammetry (DPV) was carried out with the same instrument and electrode setup under identical experimental conditions. HOMO and LUMO values were determined from the half-wave potentials in $\text{CH}_2\text{Cl}_2/\text{TBAPF}_6$ solution and calculated according to $E(\text{HOMO}/\text{LUMO}) = -5.16 \text{ eV} - E_{1/2}^{\text{ox/red}}$. It was assumed that $\text{Fc}/\text{Fc}^+ = +0.46 \text{ eV}$ vs SCE (0.1 M TBAPF₆ in CH_2Cl_2)⁵⁹ and SCE = 0.24 eV vs the standard hydrogen electrode (SHE).⁶⁰ The absolute potential of SHE was found to be 4.46 eV.⁶¹ Spectroelectrochemical experiments were performed in a specially designed sample compartment consisting of a cylindrical quartz cell, a platinum disk electrode ($\text{Ø} = 6 \text{ mm}$), a gold-covered metal (V2A) plate as the counter electrode and an Ag/AgCl pseudoreference electrode. Solvents and electrolytes were the same as those used for CV experiments and measurements were performed under argon atmosphere. Spectra were recorded with a JASCO V-570 UV/vis/NIR spectrometer in reflection mode. The vertical position of the working electrode was adjusted with a micrometer screw 100 μm above the bottom of the cell. The potential was applied by an EG & G Princeton Applied Research Model 283 potentiostat and was varied in steps of 20–100 mV.

Transient Absorption Spectroscopy. The laser system used for the femtosecond transient absorption experiments consists of an ultrafast Ti:sapphire amplifier (Spectra Physics Solstice) with a repetition rate of 1 kHz, a central wavelength of 800 nm, and a pulse duration of 100 fs. One part of the output power was used to seed a noncollinear optical parametric amplifier (Light Conversion TOPAS White) which produced the pump pulses centered at 525 nm with a duration of about 55 fs as verified by frequency-resolved optical gating measurements.⁶² A small fraction of the Ti:sapphire output was focused into a linearly moving CaF₂-plate to produce a supercontinuum between 390 and 750 nm, which acted as the probe beam. After passing the sample the probe pulses were detected via a spectrograph (Acton SP2558) with a CCD camera (Princeton Instruments Pixis 2k). A mechanical chopper, working at 500 Hz, blocks every second pump pulse, thus enabling low noise shot-to-shot-measurements, eliminating the need for a reference beam. By comparing the transmitted spectral intensity of consecutive pulses $[I(\lambda, \tau), I_0(\lambda)]$ the photoinduced change in the optical density can be directly recorded as $\Delta OD = -\log[I(\lambda, \tau)/I_0(\lambda)]$. For the measurements, pump and probe pulses were focused noncollinearly and spatially overlapped in a 500 μm flow cell with beam diameters of 40 μm and less than 30 μm , respectively, while the polarizations were set to the magic angle of 54.7°. The pump power was attenuated resulting in pulse energies of 100 nJ (**M** in toluene and CH_2Cl_2 and **P1** in CH_2Cl_2) and 260 nJ (**P1** in toluene). The relative temporal delay between pump and probe pulses was varied over a maximum range of 3.6 ns with a motorized, computer-controlled linear stage. The delay interval between two consecutive data points was 100 fs for small delay times and was increased up to 30 ps for very large delay times. The data were analyzed by a least-squares fitting algorithm. The nonlinear fit model was a multiexponential function in combination with a Heaviside step function. In case of the polymer a biexponential decay was assumed. For the monomer we used a

(59) Connelly, N. G.; Geiger, W. E. *Chem. Rev.* **1996**, *96*, 877–910.

(60) Sawyer, D. T.; Roberts, J. L. *Experimental Electrochemistry for Chemists*; Wiley-Interscience: New York, 1974; p 42.

(61) Tsiplakides, D.; Archonta, D.; Vayenas, C. G. *Top. Catal.* **2007**, *44*, 469–479.

(62) Trebino, R.; DeLong, K. W.; Fittinghoff, D. N.; Sweetser, J. N.; Krumbügel, M. A.; Richman, B. A.; Kane, D. J. *Rev. Sci. Instrum.* **1997**, *68*, 3277–3295.

sum of monoexponential rise and decay functions. Where the coherent artifact⁶³ was observable, selected data points around time zero were omitted from the fit.

OFET Fabrication. Heavily doped n-type Si substrates as the gate and thermally grown 200 nm silicon dioxide as the dielectric layer (Si-Mat) were cleaned in an ultrasonic bath with acetone and isopropanol. For device A (bottom gate/bottom contact structure), first source and drain electrodes (1 nm Ti adhesion layer/19 nm Au) were patterned using standard photolithography. The semiconductor layer was then spin-coated (1500 rpm, 60 s) on top from a 1 wt % solution of **P1** in chlorobenzene inside a nitrogen-filled glovebox. For device B (bottom gate/top contact structure), polypropylene-*co*-1-butene (12 wt % 1-butene, Aldrich) was dissolved in anhydrous decaline (cis/trans mixture, Aldrich) at 190 °C (20 mg/mL) and spin coated in air on top of the SiO₂ surface using a preheated copper chuck (2500 rpm, 60 s). The device was heated for 1 min at 200 °C in air and then transferred to the glovebox where **P1** was spin coated (1 wt % in chlorobenzene, 1500 rpm, 60 s) on top. As final layer, Au source and drain contacts (50 nm) were evaporated through a shadow mask. The as-prepared devices (A and B) were heated at 120 °C for 20 h in vacuum prior to the measurements using an Agilent Parameter Analyzer 4155C. Mobilities μ were calculated from the transfer curves in the saturation regime at a drain voltage $|V_D| = 50$ V according to eq 1

$$\sqrt{\mu_{\text{sat}}} = \frac{\partial \sqrt{I_{\text{ds}}}}{\partial V_{\text{g}}} \times \sqrt{\frac{2L}{WC_i}} \quad (1)$$

where I_{ds} is the source-drain current, V_{g} is the gate voltage, L and W are the channel length and width, respectively, and C_i is the dielectric capacitance per unit area.

Results and Discussion

Synthesis. The monomer **M** was synthesized by an improved method which gives the radical **M** free of α -H precursor impurities.³⁰ The synthetic approach to **P1** is outlined in Scheme 1. Compound **4** is prepared in analogy to a procedure established by Veciana et al.¹² A Horner–Emmons reaction of **4** and dialdehyde **6**^{56,57} in THF with KO^{*t*}Bu as base yields polymer **7**. After the reaction has completed, the reaction mixture was acidified in order to protonate PCTM anions that may have formed, because the α -H compounds are rather strong acids.⁶⁴ In the ¹H and ¹³C NMR spectra, no signals corresponding to the aldehyde group were visible whereas signals corresponding to the –CH₂P(O)(OEt)₂ group could be identified. The all-*E* configuration of the ethylene bridges was confirmed by IR, ¹H and ¹³C NMR spectroscopy: In the IR spectrum, the band at 967 cm⁻¹ indicates *E*-configuration⁶⁵ and in the ¹H NMR spectrum no signals at around 6.6 ppm corresponding to the *Z*-configuration of the vinylene bridges were visible.¹² Furthermore, in the ¹³C NMR spectra, no additional carbon signals but exactly six carbon signals corresponding to the 16 tertiary

carbon atoms in the repeating unit (2 × 4C and 2 × 2C for the triarylamine moiety, and 2 × 2C for the ethylene bridges) were found. This contrasts the findings of Veciana et al.¹² who obtained a mixture of *Z*- and *E*-isomers by applying the Horner–Emmons reaction to the monophosphonate analogue of compound **4**. In the case of polymer **7**, the formation of the *Z*-isomer might well be suppressed because of steric hindrance.

Radicalization of **7** to give **P1** was achieved by deprotonation of the α -H atoms of the PCTM moieties with an aqueous *n*-Bu₄NOH solution in THF and subsequent oxidation with *p*-chloranil according to the procedure by Veciana et al.¹² Polymer **P1** was isolated and purified by repeated dropwise addition of a concentrated THF solution of **P1** to an acetone/HCl mixture to give a dark brown precipitate that was further washed with acetone in a Soxhlet apparatus in order to remove excess *p*-chloranil and low molecular weight fractions. The completeness of the radicalization was confirmed by differential pulse voltammetry (DPV): Integration of the oxidation and reduction signal of **P1** measured in dichloromethane/tetrabutylammonium hexafluorophosphate (TBAPF₆, 0.2 M) resulted in equal values as expected for equal amounts of donor and radical moieties thus proving **P1** to be fully radicalized. Again a band at 964 cm⁻¹ was visible in the IR-spectrum, indicating *E*-configuration of the vinylene bridges.

Polymer **P1** is soluble in common organic solvents such as THF, chloroform, dichloromethane, toluene and chlorobenzene. Solid **P1** is stable for several months, and even in solution (toluene 0.3 mg/mL), it can be stored for at least 2 months under ambient conditions. No phase transition was observed with differential scanning calorimetry (DSC) measurements. Instead **P1** starts to decompose at about 250 °C. Gel permeation chromatography (GPC) performed in THF vs polystyrene standards gave an average molecular weight $\bar{M}_w = 19300$ Da ($\bar{M}_n = 11200$ Da, PDI = 1.72) corresponding to $\bar{X}_w = 17$ and $\bar{X}_n = 10$ for **P1**, whereas for the nonradicalized precursor polymer **7**, an average molecular weight $\bar{M}_w = 17100$ Da ($\bar{M}_n = 9600$ Da, PDI = 1.77) corresponding to $\bar{X}_w = 15$ and $\bar{X}_n = 9$ was found under the same experimental conditions. End group analysis of the ¹H NMR spectrum of **7** revealed polymer chains with $\bar{X}_n = 12$ terminated by diethylphosphonate groups on both ends as depicted in Scheme 1. The latter value seems to be more reliable because with GPC only rough estimates can be obtained. The small differences between the molecular weight data of **P1** and of **7** show that the radicalization and workup did not influence the chain length distribution to a significant extent.

Optical Properties. Absorption spectra of **P1** measured in dichloromethane and toluene are displayed in Figure 2a together with the absorption spectra of the reference molecule **M**. Energies of absorption bands $\tilde{\nu}$ and corresponding molar extinction coefficients ϵ are listed in Table 1.

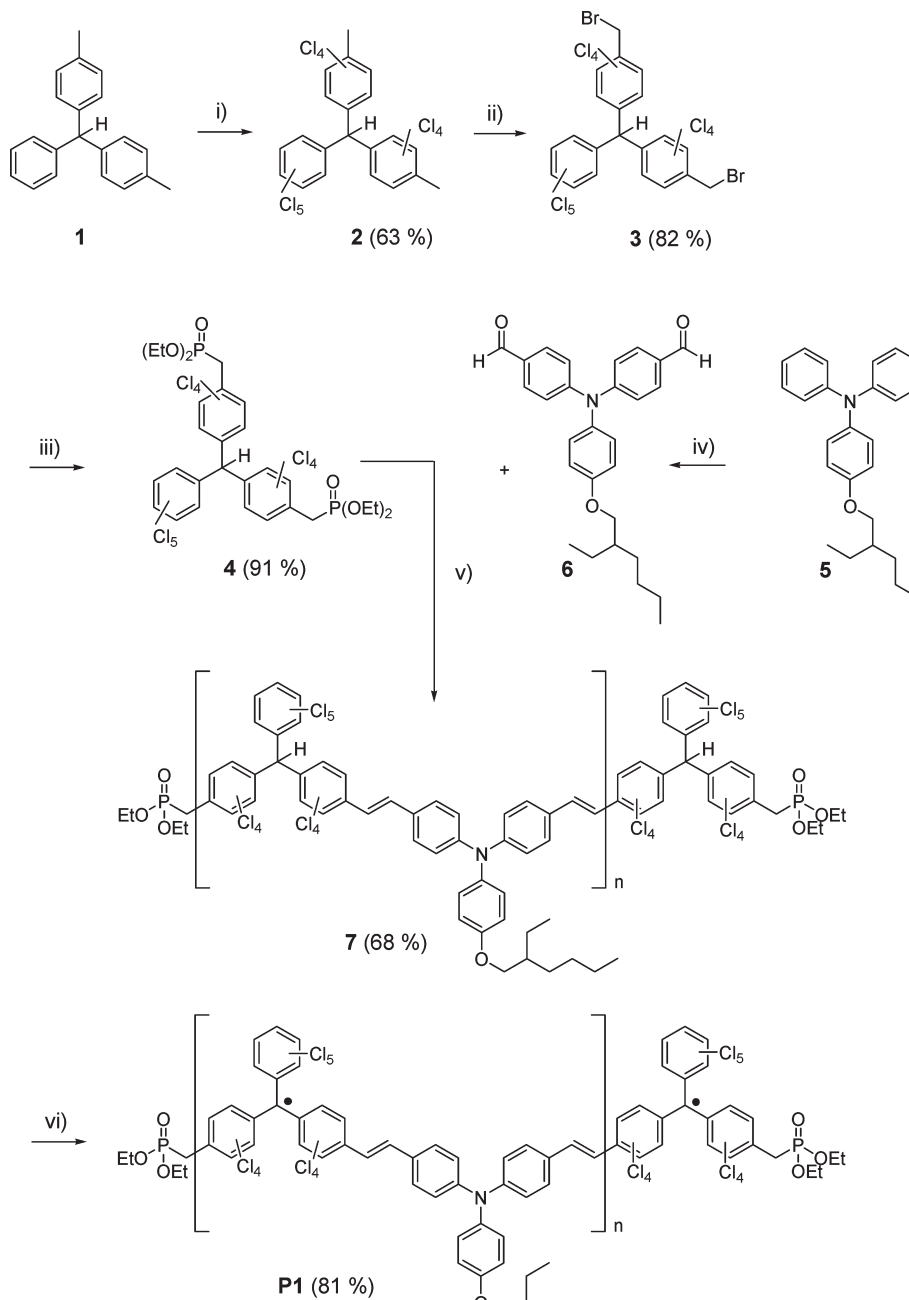
Absorption bands of **P1** resemble those of **M** and can be assigned as follows: Bands around 34 500 cm⁻¹

(63) Ekvall, K.; van der Meulen, P.; Dhollande, C.; Berg, L.-E.; Pommeret, S.; Naskrecki, R.; Mialocq, J.-C. *J. Appl. Phys.* **2000**, *87*, 2340–2353.

(64) Ballester, M.; Riera, J.; Castañer, J.; Badía, C.; Monsó, J. M. *J. Am. Chem. Soc.* **1971**, *93*, 2215–2225.

(65) Kang, I.-N.; Hwang, D.-H.; Shim, H.-K.; Zyung, T.; Kim, J.-J. *Macromolecules* **1996**, *29*, 165–169.

Scheme 1. Synthesis of P1



(i) S_2Cl_2 , AlCl_3 , SO_2Cl_2 , reflux, 8 h; (ii) NBS, AIBN, CCl_4 , reflux, 60 h; (iii) $\text{P}(\text{OEt})_3$, reflux, 2 h; (iv) POCl_3 , DMF, 100°C , 15 h; (v) KO^tBu , THF, r.t., 3 h; (vi) (1) $n\text{-Bu}_4\text{NOH}$ (1.5 M in H_2O), THF, r.t., 1 h; (2) *p*-chloranil, r.t., 21 h.

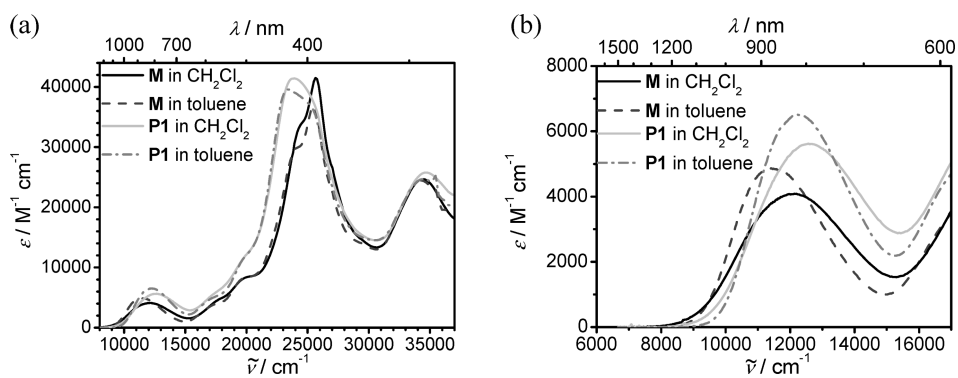


Figure 2. (a) Absorption spectra of M and P1 in CH_2Cl_2 and toluene; (b) enhanced IV-CT bands from panel a.

Table 1. Absorption Band Energies of **M** and **P1** in CH₂Cl₂ and Toluene Solution and a Thin Film of **P1**

$\tilde{\nu}$ (cm ⁻¹) (ϵ (M ⁻¹ cm ⁻¹) ^b)				
M (CH ₂ Cl ₂) ^a	P1 (CH ₂ Cl ₂)	M (toluene)	P1 (toluene)	P1 (thin film)
34 500 (24 700)	34 700 (25 800)	34 200 (24500)	34 500 (24 700)	34 200
25 600 (41 500)		25 500 (36800)	25 300 (36 900)	25 100
24 500 (34 000)	23 900 (41 400)	24 200 (29900)	23 400 (39 600)	23 300
20 200 (8500)	19 600 (1100)	20 000 (8400)	20 200 (12 400)	20 200
17 900 (4900)	17 200 (5500)	17 400 (3900)	17 400 (5100)	17 200
12 100 (4100)	12 600 (5600)	11 400 (4900)	12 200 (6500)	11 800

^a Values differ from previously published data^{29,30} because those were measured on a batch of **M** that still contained a small fraction of nonradicalized PCTM moieties, and thus a lower intensity for all bands was observed. ^b per monomer unit.

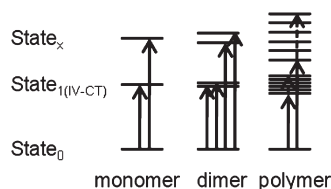


Figure 3. Band broadening due to exciton coupling interactions between adjacent molecular units in polymers.

correspond to localized triarylamine transitions⁶⁶ and bands between 25 600 and 17 200 cm⁻¹ belong to the PCTM radical moiety.⁶⁷ The band of particular interest is the IV-CT band located around 12 000 cm⁻¹.³⁰ This transition is somewhat higher in energy for **P1** (12 600 cm⁻¹, dichloromethane) than for **M** (12 100 cm⁻¹, dichloromethane) which can be explained by the weaker donor strength of the triarylamine moiety in **P1** compared to **M**. This interpretation is also supported by the differing oxidation potentials of **P1** and **M** (see cyclic voltammetry). A hypsochromic shift of the IV-CT band with decreasing donor strength of the triarylamine moiety was also found for a series of analogous compounds with biphenyl spacer.²⁸ The shift and broadening of the IV-CT bands in going from the nonpolar solvent (toluene) to the polar solvent (dichloromethane) is similar for **M** and **P1** (Figure 2b) and has been explained previously.^{29,30} The full-width at half-maximum values are $\tilde{\nu}_{1/2} = 3900$ cm⁻¹ and 3300 cm⁻¹ for **M** and 3800 cm⁻¹ and 3400 cm⁻¹ for **P1** in dichloromethane and toluene, respectively. Similarly to the smaller shift between $\tilde{\nu}_{\max,IVCT}$ (dichloromethane) and $\tilde{\nu}_{\max,IVCT}$ (toluene) for **P1** (400 cm⁻¹) compared to **M** (700 cm⁻¹) the difference in $\tilde{\nu}_{1/2}$ in these two solvents is also smaller for **P1** than for **M**. However, the fact that $\tilde{\nu}_{1/2}$ values of **M** and **P1** are still very similar to each other in the respective solvents indicates that the IV-CT transition in **P1** is confined to one repeating unit. In contrast to the close resemblance of the IV-CT bands of **M** and **P1**, the absorption maximum of **P1** at ca. 24 000–26 000 cm⁻¹ differs significantly from that of **M** in that it is broadened and shifted to the red by 1700 cm⁻¹ in dichloromethane. The seeming contradiction can be explained by exciton splitting, which stems from the dipole–dipole interaction of transition moments localized

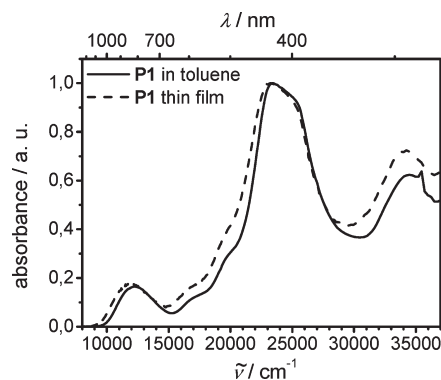


Figure 4. Normalized absorption spectra of **P1** in toluene and as thin film spin-coated from a toluene solution onto a quartz plate.

on adjacent molecular units (Figure 3). With increasing band intensity the exciton coupling energy ϵ rises, because it is proportional to the square of the transition moment μ_{ab} of the individual monomer: $\epsilon \approx \mu_{ab}^2$.⁶⁸ Since the transitions at 24 000–26 000 cm⁻¹ have much higher intensities than the IV-CT band one can qualitatively expect a much higher exciton coupling of the former transitions and thus a significant broadening of the high-energy bands.

The solid-state absorption spectrum of **P1** spin-coated from toluene onto a quartz plate reveals the same spectral shape as the toluene solution spectrum (Figure 4) except for a small red shift commonly observed for solid-state spectra because of interchain interactions^{69–72} that are, however, weak in films of **P1**. The same solid-state spectrum is also obtained, when **P1** is spin-coated from chlorobenzene under the same conditions. Annealing of as-prepared films in air at 110 °C for 30 min did not alter the spectrum significantly. This points to a pronounced air stability and the amorphous character of the film, because a higher ordering, which can be induced by annealing, would shift the absorption edge

(66) Amthor, S.; Noller, B.; Lambert, C. *Chem. Phys.* **2005**, *316*, 141–152.

(67) Ballester, M. *Adv. Phys. Org. Chem.* **1989**, *25*, 267–445.

(68) Kasha, M. *Physical Processes in Radiation Biology*; Augenstein, L., Mason, R., Rosenberg, B., Eds.; Academic Press: New York, 1964; pp 23–42.

(69) Blouin, N.; Michaud, A.; Gendron, D.; Wakim, S.; Blair, E.; Neagu-Plesu, R.; Belletête, M.; Durocher, G.; Tao, Y.; Leclerc, M. *J. Am. Chem. Soc.* **2007**, *130*, 732–742.

(70) Mikroyannidis, J. A.; Sharma, G. D.; Sharma, S. S.; Vijay, Y. K. *J. Phys. Chem. C* **2010**, *114*, 1520–1527.

(71) Mühlbacher, D.; Scharber, M.; Morana, M.; Zhu, Z.; Waller, D.; Gaudiana, R.; Brabec, C. *Adv. Mater.* **2006**, *18*, 2884–2889.

(72) Yue, W.; Zhao, Y.; Tian, H.; Song, D.; Xie, Z.; Yan, D.; Geng, Y.; Wang, F. *Macromolecules* **2009**, *42*, 6510–6518.

Table 2. Oxidation and Reduction Potentials, HOMO and LUMO Values and Electrochemical (E_g) and Optical (E_g^{opt}) Band Gaps of **M and **P1****

	$E_{1/2}^{\text{ox}}$ (mV) ^a	$E_{1/2}^{\text{red}}$ (mV) ^a	HOMO (eV)	LUMO (eV)	E_g (eV) ^b	E_g^{opt} (eV) ^c	E_g^{BJ} (eV) ^d
M CH ₂ Cl ₂ toluene	+240 ³⁰	-670 ^{1,30}	-5.40	-4.49	0.91	1.13	1.00
P1 CH ₂ Cl ₂ toluene	+340	-690	-5.50	-4.47	1.03	1.19	1.24
						1.23	1.24

^a Half-wave potentials vs Fc/Fc⁺: **P1**, CH₂Cl₂/TBAPF₆ 0.2 M, $\nu = 100 \text{ mV s}^{-1}$; **M**, CH₂Cl₂/TBAPF₆ 0.1 M, $\nu = 250 \text{ mV s}^{-1}$. ^b $E_g = \text{LUMO} - \text{HOMO}$. ^c E_g^{opt} is determined from the onset absorptions. ^d $E_g^{\text{BJ}} = \Delta G^{00}$ (see Figure 1) is determined by a Bixon–Jortner band shape analysis of the IV-CT band, see ref 29.

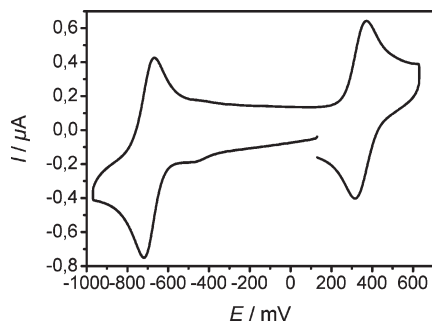


Figure 5. Cyclic voltammogram of **P1** in CH₂Cl₂/TBAPF₆ (0.2 M), $\nu = 100 \text{ mV s}^{-1}$.

farther to the red because of more effective interchain interactions.^{73–75}

The optical band gaps E_g^{opt} as determined from the onset absorptions (Table 2) are slightly smaller for **M** (1.13 eV in dichloromethane, 1.15 eV in toluene) than for **P1** (1.19 eV in dichloromethane, 1.23 eV in toluene, 1.17 eV in solid state) consistent with the higher energy of the IV-CT transition of **P1**.

Summarizing the optical properties **P1** is a low-band-gap MV polymer, that forms air- and temperature-stable, amorphous films and shows IV-CT characteristics similar to **M**.

Cyclic Voltammetry. Half wave potentials $E_{1/2}$ of oxidation and reduction processes were determined by cyclic voltammetry in dichloromethane/TBAPF₆ (0.2 M) with potentials being referenced against ferrocene (Fc/Fc⁺). The oxidation of the amine moiety and the reduction of the PCTM radical of **P1** occur at $E_{1/2}^{\text{ox}} = +340 \text{ mV}$ and at $E_{1/2}^{\text{red}} = -690 \text{ mV}$, respectively (Figure 5, Table 2). Both signals are chemically fully reversible as confirmed by multisweep experiments in a thin layer whereupon the signals did not alter significantly. Under semi-infinite conditions the peak separation ΔE_p decreases during subsequent scans from 82 mV (oxidation) and 72 mV (reduction) at the beginning to 33 and 32 mV, respectively, after 32 scans. This observation indicates adsorption of **P1** on the surface of the working electrode with increasing number of voltammetric cycles, which implies a transition from semi-infinite conditions (theoretical value for reversible one-electron processes at 25 °C:

$\Delta E_p = 58 \text{ mV}^{76}$) to thin-layer conditions (theoretical value for reversible processes: $\Delta E_p = 0 \text{ mV}^{77}$). Note that in practice ΔE_p values may be substantially larger than the theoretical values due to voltage drops of uncompensated solution resistance. The full-width at half-maximum of the signals determined from DPV measurements are about 100 mV for both **P1** and **M**, which shows that the redox centers behave as independent units with negligible inhomogeneous distribution of redox potentials in the polymer **P1**. In comparison to the oxidation potential of **M** ($E_{1/2}^{\text{ox}} = +240 \text{ mV}$)³⁰ the oxidation of **P1** occurs at considerably higher potential, whereas the reduction potentials are almost identical ($E_{1/2}^{\text{red}}$ (**M**) = -670 mV).³⁰ These findings agree well with our previous results: The oxidation potentials of triarylamine molecules strongly depend on the donor/acceptor strength of the substituents,⁶⁶ whereas the reduction potential of the PCTM radical moiety is nearly independent of the donor strength of the amine moiety if the two centers (C[•] and N) are connected by the same spacer.²⁹ Thus the presence of two PCTM radical acceptors next to the amine moiety shifts the oxidation of **P1** to higher potentials as compared to **M**.

The important values for the application of **P1** in electronic devices are the HOMO and LUMO values, which were determined from the half-wave potentials of the oxidation and the reduction process, respectively (see Experimental Section). Even though usually onset potentials are taken for the estimation of the electrochemical band gaps of polymers based on the work of Brédas in 1983,⁷⁸ we used the half-wave potentials for the following reason: The half-wave potential is the thermodynamic quantity that is measured (relative to potentials of reference electrodes or an internal redox couple such as Fc/Fc⁺) as the potential needed to bring the Fermi level of the electrode to the free energy of a 1:1 mixture of reduced and oxidized species (= formal potential). This free energy can be set as the HOMO (or LUMO) energy provided differences of solvation and reorganizational effects of reduced and oxidized species are negligible or cancel out. These constrictions are important to mention because the HOMO/LUMO energies refer to vertical ionization and electron affinity values while redox potentials refer to adiabatic ionization and electron affinities.⁷⁹ In cases where the determination of a

(73) Bürgi, L.; Turbiez, M.; Pfeiffer, R.; Bienewald, F.; Kirner, H.-J.; Winnewisser, C. *Adv. Mater.* **2008**, *20*, 2217–2224.

(74) Kietzke, T.; Hörhold, H.-H.; Neher, D. *Chem. Mater.* **2005**, *17*, 6532–6537.

(75) Völker, S. F.; Uemura, S.; Limpinsel, M.; Mingebach, M.; Deibel, C.; Dyakonov, V.; Lambert, C. *Macromol. Chem. Phys.* **2010**, *211*, 1098–1108.

(76) Bard, A. J.; Faulkner, L. R. *Electrochemical Methods*, 2nd ed.; John Wiley & Sons: New York, 2001; p 241.

(77) Bard, A. J.; Faulkner, L. R. *Electrochemical Methods*, 2nd ed.; John Wiley & Sons: New York, 2001; p 456.

(78) Brédas, J. L.; Silbey, R.; Boudreaux, D. S.; Chance, R. R. *J. Am. Chem. Soc.* **1983**, *105*, 6555–6559.

(79) Schmidt, A.; Anderson, M. L.; Armstrong, N. R. *J. Appl. Phys.* **1995**, *78*, 5619–5625.

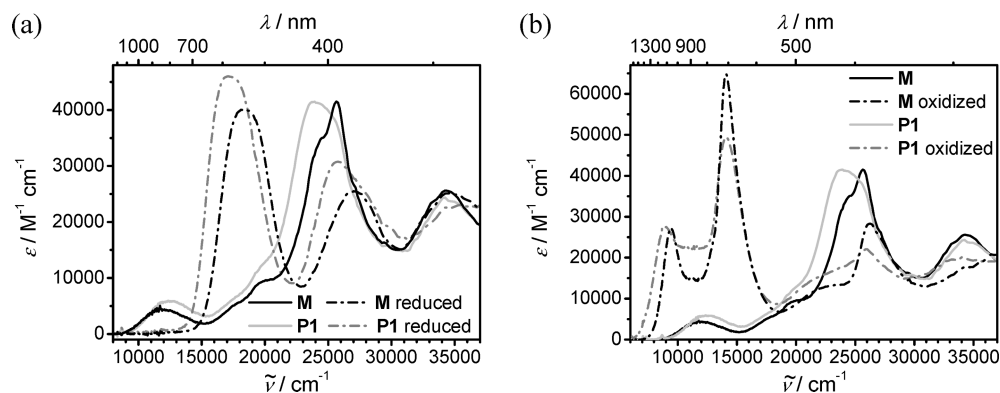


Figure 6. Absorption spectra of **M** (0.2 mM) and **P1** (0.2 mM) in $\text{CH}_2\text{Cl}_2/\text{TBAPF}_6$ (0.2 M) in their (a) fully reduced and (b) fully oxidized states together with the spectra of the neutral species.

half-wave potential is impossible because of strongly overlapping signals, for example, in polymers, the onset potential may be used instead.⁷⁸ The HOMO and LUMO energies of **P1** determined from the half-wave potentials are -5.50 and -4.47 eV, respectively, resulting in an electrochemical band gap of $E_g = 1.03$ eV (Table 2). These values are perfectly suitable for the application of **P1** in an ambipolar OFET device with Au contacts, since the Au work function ($4.7\text{--}5.2$ eV)^{80,81} is close to these values and thus charge carrier injection barriers for both holes and electrons should be small. Moreover the low lying HOMO and LUMO make **P1** stable against redox reactions with wet air.⁸²

For comparison HOMO and LUMO values of **M** were determined from the CV of ref 30 in the same way as it was done for **P1** giving -5.40 eV (HOMO) and -4.49 eV (LUMO) (Table 2). For both **M** and **P1** the optical band gap energies E_g^{opt} as determined from the absorption onsets⁸³ of the solution spectra (**P1**: 1.19 eV in CH_2Cl_2 , **M**: 1.13 eV in CH_2Cl_2) are larger than the electrochemical E_g values (Table 2). The deviation is only slightly smaller if the absorption onsets are determined from the spectra of neutral species recorded during spectroelectrochemical measurements (see below) under experimental conditions (supporting electrolyte solution) similar to those of the CV measurements, which gave $E_g^{\text{opt}} = 1.17$ eV for **P1** and $E_g^{\text{opt}} = 1.13$ eV for **M**. In solid state (thin film on quartz plate) $E_g^{\text{opt}} = 1.17$ eV for **P1**. In general, the spectra in pure CH_2Cl_2 only marginally deviate from those with electrolyte. These findings suggest that the deviation between E_g^{opt} and E_g is not caused by medium effects. In theory, one would expect that E_g^{opt} is smaller than E_g because of the exciton binding energy. In **M** and **P1**, this exciton binding energy might be small because of the explicit CT character of the lowest-energy transition which already requires a spatial separation of hole and electron. In a previous work, we evaluated the band gap

of **M** in CH_2Cl_2 by a Bixon-Jortner analysis, in which a Golden Rule type equation is fitted to the IV-CT band in order to obtain $\Delta G^{00} = E_g^{\text{BJ}}$ (see Figure 1).²⁹ For **M** in toluene and for **P1** we performed an analogous analysis in this work which rests on the assumption that the broadening of the IV-CT band of the polymer due to exciton coupling is negligible (see above). In fact, excellent agreement between E_g^{opt} and E_g^{BJ} is found for **M** in toluene and for **P1** in both solvents (see Table 2). This analysis excludes reorganizational effects to be the source of the deviations between optically and electrochemically determined band gaps. The major source for the discrepancies might still be ion pairing effects in the apolar CH_2Cl_2 solution which lowers the ionization energy and electron affinity in the electrochemical experiments. The overall good agreement of E_g^{opt} and E_g^{BJ} shows that the exciton binding energy is small in **P1**. However, given the systematic inaccuracy of the methods for determining the band gap we cannot rule out exciton binding energies in the order of 100–200 mV.

Spectroelectrochemistry. By spectroelectrochemistry we obtained the absorption spectra of oxidized triarylamine donor $\text{D}^{+\bullet}$ and reduced PCTM acceptor A^- moieties independently. Since the IV-CT band is caused by an ET from the triarylamine to the PCTM radical moiety (Figure 1), the sum of the spectra of $\text{D}^{+\bullet}$ and A^- should approximately give the transient absorption profile of the IV-CT state (lowest excited state), with exception of those contributions that are due to interactions between $\text{D}^{+\bullet}$ and A^- , i.e., the IV-CT band itself. Thus, the spectra obtained by spectroelectrochemistry may help for the interpretation of transient absorption spectra (see below). In Figure 6, the absorption spectra of reduced and oxidized **M** and **P1** are displayed together with the absorption spectra of the neutral species.

For both, reduced **M** and reduced **P1**, an intense broad band (**M**: $18\,400\text{ cm}^{-1}$, $\epsilon = 40\,100\text{ M}^{-1}\text{ cm}^{-1}$ and **P1**: $17\,100\text{ cm}^{-1}$, $\epsilon = 46\,000\text{ M}^{-1}\text{ cm}^{-1}$), typical of PCTM anions^{12,29,84} is observed (Figure 6a). The radical band of the neutral species at around $25\,000\text{ cm}^{-1}$ decreased and is

(80) Zaumseil, J.; Sirringhaus, H. *Chem. Rev.* **2007**, *107*, 1296–1323.

(81) McNeill, C. R.; Abrusci, A.; Zaumseil, J.; Wilson, R.; McKiernan, M. J.; Burroughes, J. H.; Halls, J. J. M.; Greenham, N. C.; Friend, R. H. *Appl. Phys. Lett.* **2007**, *90*, 193506.

(82) de Leeuw, D. M.; Simenon, M. M. J.; Brown, A. R.; Einerhand, R. E. F. *Synth. Met.* **1997**, *87*, 53–59.

(83) Gierschner, J.; Cornil, J.; Egelhaaf, H. J. *Adv. Mater.* **2007**, *19*, 173–191.

(84) Sporer, C.; Ratera, I.; Ruiz-Molina, D.; Zhao, Y. X.; Vidal-Gancedo, J.; Wurst, K.; Jaitner, P.; Clays, K.; Persoons, A.; Rovira, C.; Veciana, J. *Angew. Chem., Int. Ed.* **2004**, *43*, 5266–5268.

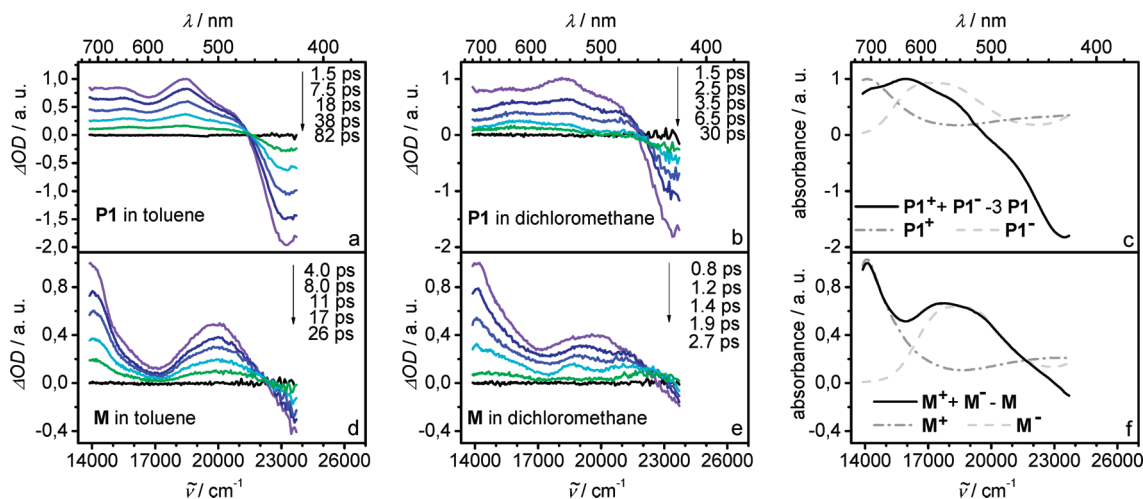


Figure 7. Normalized transient absorption spectra of **P1** in (a) toluene and (b) CH_2Cl_2 and of **M** in (d) toluene and (e) CH_2Cl_2 together with the sum of the spectra of reduced (P1^- , M^-) and oxidized (P1^+ , M^+) (c) polymer and (f) monomer minus their respective ground state absorption (three times for **P1**) obtained by spectroelectrochemistry in $\text{CH}_2\text{Cl}_2/\text{TBAPF}_6$ (0.2 M). All spectra are normalized to the absorption maximum. In the transient spectra, the data points of the black curves were recorded before time zero.

blue-shifted (**M**: $27\,000\text{ cm}^{-1}$, $\epsilon = 25\,500\text{ M}^{-1}\text{ cm}^{-1}$; **P1**: $25\,800\text{ cm}^{-1}$, $\epsilon = 30\,800\text{ M}^{-1}\text{ cm}^{-1}$) in the spectra of the reduced species. In addition, the IV-CT band is absent, because there is no ET possible upon excitation of the PCTM anion. The higher intensity of the bands of reduced **P1** as compared to those of **M** results from the additional PCTM radical moiety attached to each polymer chain end (Chart 1).

In the spectra of oxidized **M** and **P1** (Figure 6b) a sharp and intense band at $14\,100\text{ cm}^{-1}$ (**M**: $\epsilon = 64\,700\text{ M}^{-1}\text{ cm}^{-1}$; **P1**: $\epsilon = 49\,400\text{ M}^{-1}\text{ cm}^{-1}$) belonging to the triarylamine radical cation^{29,66} and a new IV-CT band at $9\,500\text{ cm}^{-1}$ ($\epsilon = 27\,200\text{ M}^{-1}\text{ cm}^{-1}$) for **M** and at $8\,900\text{ cm}^{-1}$ ($\epsilon = 27\,500\text{ M}^{-1}\text{ cm}^{-1}$) for **P1** is visible. The latter arises from an ET from the PCTM radical to the triarylamine radical cation center.²⁹ Thus, donor and acceptor functionalities of the moieties exchange in the oxidized species and the formerly weaker donor of neutral **P1** is now a stronger acceptor compared to the corresponding moiety of **M**, which causes the red shift of the IV-CT band of oxidized **P1** relative to the IV-CT band of oxidized **M**. Similar to the spectra of reduced **M** and **P1** the radical band of the neutral spectrum at around $25\,000\text{ cm}^{-1}$ decreased and is blue-shifted (**M**: $26\,300\text{ cm}^{-1}$, $\epsilon = 28\,300\text{ M}^{-1}\text{ cm}^{-1}$, shoulder at $22\,900\text{ cm}^{-1}$; **P1**: $25\,900\text{ cm}^{-1}$, $\epsilon = 22\,100\text{ M}^{-1}\text{ cm}^{-1}$ shoulder at $22\,100\text{ cm}^{-1}$) in the spectra of the oxidized species.

Transient Absorption Spectroscopy. To investigate the dynamics of photoinduced ET phenomena, we performed fs-pump-probe transient absorption spectroscopy. Polymer **P1** and monomer **M** dissolved in toluene and dichloromethane were excited at 525 nm and their transient spectra were recorded with femtosecond time resolution. In toluene, the transient spectra of **P1** show two bands at $18\,300$ and $15\,200\text{ cm}^{-1}$ (Figure 7a), which correspond to characteristic transitions of the anion (P1^-) and radical cation (P1^+), respectively, as was proved by comparison with spectroelectrochemistry (Figure 7c) although the bands in those experiments appear at somewhat lower

energy ($17\,100$ and $14\,100\text{ cm}^{-1}$). The transient band at $15\,200\text{ cm}^{-1}$ shifts to $15\,600\text{ cm}^{-1}$ at longer delay times. A ground state bleaching is observed at $23\,100\text{ cm}^{-1}$. In dichloromethane, initially two bands at $18\,100$ and $15\,400\text{ cm}^{-1}$ are observed similar to those in toluene. At longer delay times, the bands in dichloromethane shift to $18\,500\text{ cm}^{-1}$ and $15\,900\text{ cm}^{-1}$ (Figure 7b). The reason for the band shifts in both solvents is presently unclear. In dichloromethane, the spectral shape at longer times resembles that of the sum of oxidized (P1^+) and reduced (P1^-) polymer minus three times the ground-state absorption of neutral **P1** obtained from spectroelectrochemistry (Figure 7c). The enlarged intensity of the ground-state bleaching cannot be explained yet.

Almost no spectral shift with time is found for the monomer **M** in toluene (Figure 7d). Transient bands are observed at $20\,000$ and $14\,000\text{ cm}^{-1}$. In dichloromethane, these bands are located at $19\,600$ and $14\,100\text{ cm}^{-1}$ (Figure 7e). Comparison of the absorption profile of the sum of the spectra of M^- and M^+ minus **M** obtained by spectroelectrochemistry (Figure 7f), which exhibits two bands at $17\,700$ and $14\,100\text{ cm}^{-1}$, with the initial transient spectra of **M** in both solvents shows again qualitative similarity. The differences between the transient spectra and the sum of the spectroelectrochemistry spectra are due to interactions between the oxidized radical donor (D^+) and the reduced acceptor (A^-) in the excited IV-CT state of monomer **M** and polymer **P1**. Nevertheless, the optically induced ET process is unambiguously identified for both **P1** and **M**.

By multiexponential fits, time constants τ were extracted from the decay curves at different wavelengths in the spectral region of the anion and radical cation band, respectively, which are compatible with the time constants extracted from the ground-state bleaching. The time constants somewhat vary with wavelength (Table 3), which reflects the error of the measurements and the model used for their analysis. The decay curves of **P1** and **M** in dichloromethane and toluene are depicted in

Table 3. Time Constants τ and Amplitudes a for **P1** and **M** at Selected Wavelengths

	P1 (toluene)				P1 (dichloromethane)			
	540 nm	560 nm	625 nm	665 nm	540 nm	560 nm	625 nm	665 nm
τ_2 (ps)	20	21	19	15	2.5	2.6	2.6	2.3
$a_2/\Delta OD (\times 10^{-3})$	19	15	13	13	13	11	9.7	10
τ_3 (ps)	69	80	78	60	78	79	51	63
$a_3/\Delta OD (\times 10^{-3})$	9.9	7.3	8.1	9.6	0.75	0.88	0.93	0.46

	M (toluene)				M (dichloromethane)			
	500 nm	520 nm	700 nm	720 nm	500 nm	520 nm	700 nm	720 nm
τ_1 (ps)	1	0.6	1	1	0.4	0.6	0.5	0.4
τ_2 (ps)	13	13	13	12	0.7	0.6	0.6	0.6

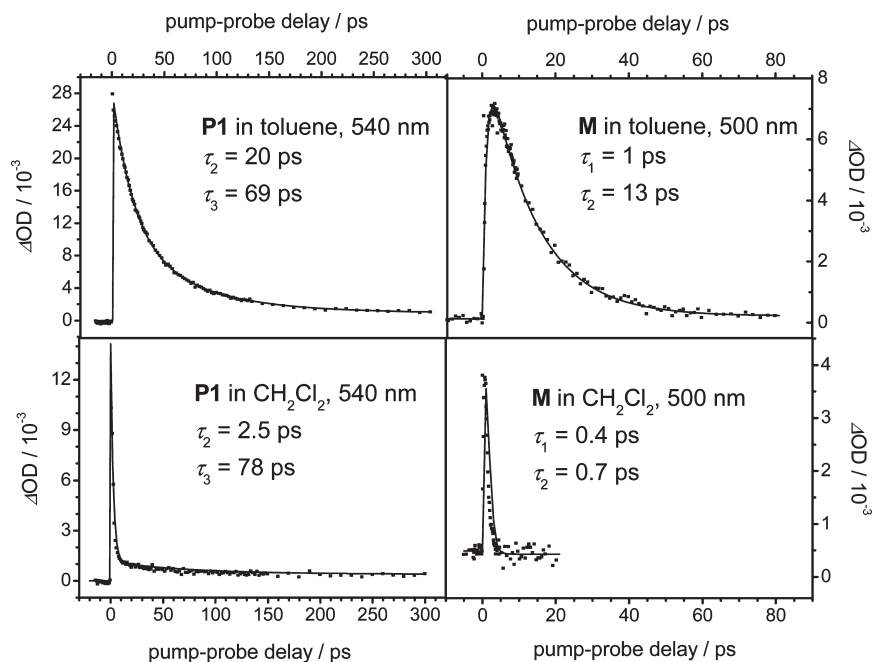


Figure 8. Experimental and fitted decay curves of **P1** and **M** in toluene and dichloromethane at selected wavelengths at a pump wavelength of 525 nm.

Figure 8. For **P1** in toluene, we found a biexponential decay with two time constants $\tau_2 \approx 20$ ps and $\tau_3 \approx 70$ ps. However, in dichloromethane, τ_2 is much smaller (≈ 2.5 ps), whereas the larger time constant τ_3 is hardly affected by the solvent (≈ 70 ps). This indicates that the smaller time constant is associated with the decay of the IV-CT state to the ground state. This decay is faster in more polar solvents because of a Marcus inverted region effect, as was found for a compound very similar to **M**.⁵³ The larger time constant probably corresponds to a structural or electronic transformation within the polymer excited state. Much in contrast, for **M**, only one short time constant, $\tau_2 \approx 13$ ps in toluene and $\tau_2 \approx 0.6$ ps in dichloromethane, is found as well as a time constant for the rise of the IV-CT state, $\tau_1 \approx 1$ ps in toluene and $\tau_1 \approx 0.5$ ps in dichloromethane. The observed rise time likely refers to the solvent dynamic modulated ET process, in good agreement with values obtained recently.⁵³

A schematic interpretation of the above results is given in Figure 9: We assume that no bimolecular or multiphotonic processes play a significant role, as we found no influence of the pump power on the transient spectra dynamics. Because of the polyradical character **P1** may

adopt different spin multiplicities in the ground and excited state. For simplicity, we restrict our discussion to the interaction of two spin bearing units, that is, to triplets and singlets. However, we stress that states of higher multiplicity might be involved. The spin–spin interaction in the ground state is expected to be quite weak, because PCTM–bridge–PCTM with shorter bridges than the triarylamine in **P1** already shows weak interactions.³⁶ In State₀ (see Figure 9), the unpaired electrons of the PCTM radical moieties (A^{\bullet}) either have α or β spin. Thus in an $[A^{\bullet}-D-A^{\bullet}]$ moiety, where D denotes the triarylamine moiety, the two spins can form either a triplet state or a singlet state. These states are anticipated to be almost degenerate. Upon excitation of **P1** the IV-CT states—singlet and triplet—are populated from higher-lying excited singlet and triplet states. The transient spectra of both triplet and singlet IV-CT states are expected to be very similar. The decay of the IV-CT states to the respective ground states (triplet and singlet) occurs approximately with τ_2 and no differences in the decay kinetics depending on the different spin states are expected. Thus, the long time constant τ_3 cannot result from this kinetic scheme. For comparison, population

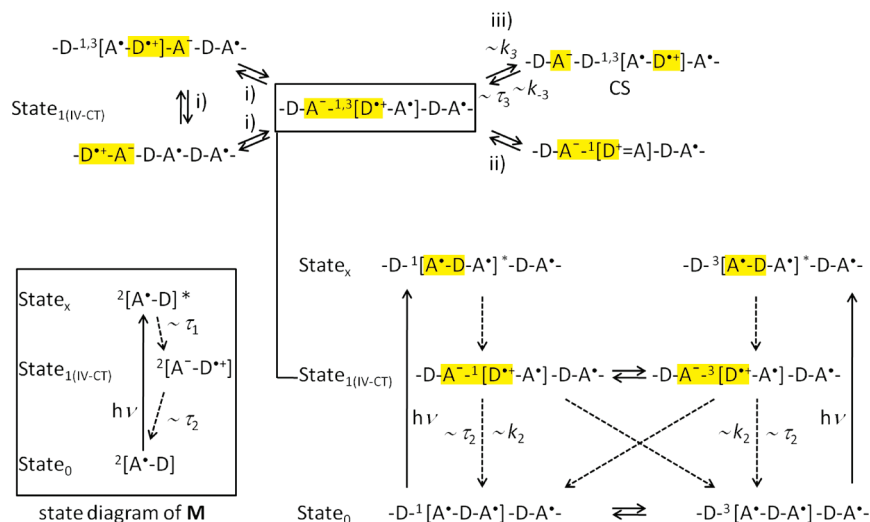


Figure 9. State diagram of **M** (box on the left side) and of **P1**. D, triarylamine moiety; A[•], PCTM radical moiety; excitons are marked in yellow.

and decay of the IV-CT state of **M** is also depicted in Figure 9 (left side), which exclusively includes doublet states. However, for **P1**, several transformations of the IV-CT state are conceivable as depicted in the upper part of Figure 9: The exciton may migrate by electron or hole transfer via an electron-deficient or electron-rich bridge. In that case, ET is identical to an excitation energy transfer (EET) (processes i). Because these newly formed states are practically identical to the primarily formed IV-CT state with identical decay dynamics, they cannot account for the third time constant, τ_3 . Furthermore, the structure of **P1** could undergo structural relaxation into a quinoid form by combination of two adjacent radicals (process ii), which would result in the planarization of the polymer backbone. This is unlikely because of sterically demanding *ortho*-chlorine atoms. Another possible transformation of the IV-CT state could be the hole transfer from D^{2+} to D (or electron transfer from D to D^{2+}) via neutral A^{\bullet} to give the charge separated species CS (process iii). Although the transient spectra of CS should be quite similar to those of the IV-CT state $State_1$ (except for the absence of the D^{2+}/A^- interaction), the decay to the $State_0$ should only be possible via back electron transfer, i.e., via the IV-CT state, thus making the back electron transfer to the IV-CT state the rate-limiting step. We assume that this process accounts for the slow decay component τ_3 , which represents an averaged time constant for back electron transfer from next nearest neighbors and those even farther apart. Although charge separation per se is an endergonic process, a reduced exciton binding energy in $State_1(IV-CT)$ of **P1** (see above) may result in an equilibrium of IV-CT state and CS state. In fact, a kinetic analysis⁸⁵ involving the $^1[State_0]$, $^1[State_1]$, and $^1[CS]$ species of **P1** ($^1[State_1] \rightarrow ^1[State_0]$, $^1[State_1] \rightarrow ^1[CS]$), with the relative amplitudes and lifetimes a_2/τ_2 and a_3/τ_3 yields the rate constants k_2 , k_3 , and k_{-3} (Figure 9). In toluene, k_2 is ca. $4 \times 10^{10} \text{ s}^{-1}$, k_3 is ca. $1 \times 10^{10} \text{ s}^{-1}$, and k_{-3} is ca. $2 \times 10^{10} \text{ s}^{-1}$. This gives an excited state equilibrium

constant $K = k_3/k_{-3} \approx 0.5$. In dichloromethane, k_2 is ca. $4 \times 10^{11} \text{ s}^{-1}$, k_3 is ca. $2.5 \times 10^{10} \text{ s}^{-1}$, and k_{-3} is ca. $2 \times 10^{10} \text{ s}^{-1}$, giving $K \approx 1.4$. The K values on the order of 1 suggest that both the IV-CT state and the CS state have almost the same free energy, which is in agreement with a very small exciton binding energy. A reason for this might be that in the CS state spin–spin interactions of three adjacent spin bearing centers ($2 \times A^{\bullet}$ and $1 \times D^{2+}$) lower the free energy of this state, which would normally be expected to be higher in energy than the IV-CT state. Further analysis of model compounds will be necessary to support the above made hypothesis.⁹³

Field-Effect Transistors. Field-effect transistor devices allow to measure electron and hole mobilities of bulk materials in a film separately. MV polymers such as **P1** may show ambipolar behavior. In order to assess the charge transport properties we fabricated field-effect transistors in two different device configurations: For device A, a bottom contact/bottom gate (BC/BG) structure with SiO_2 as gate dielectric and Au source/drain contacts was chosen. For device B a top contact/bottom gate (TC/BG) structure with an additional organic insulating layer of polypropylene-*co*-1-butene (PPcB) placed upon the SiO_2 surface and Au source/drain contacts evaporated on top of the **P1** layer was used. The staggered configuration (device B) offers the advantage of enhanced charge injection.⁸⁶ The use of the PPcB layer aims at the suppression of electron trapping often encountered at SiO_2 surfaces⁸⁷ and the lowering of energetic disorder at the semiconductor/insulator interface, which is achieved with low-permittivity materials ($2.1 \leq k \leq 2.3$) like PPcB.⁸⁸

In Table 4, device configurations and mobilities calculated in the saturation regime are listed. Interestingly, in device A the hole mobility is lower than the electron mobility in contrast to what is anticipated for semiconductor

(85) Mauser, H.; *Formale Kinetik*; Bertelsmann Universitätsverlag: Düsseldorf, Germany, 1974; p 74.

(86) Street, R. A.; Salleo, A. *Appl. Phys. Lett.* **2002**, *81*, 2887–2889.
 (87) Chua, L.-L.; Zaumseil, J.; Chang, J.-F.; Ou, E. C.-W.; Ho, P. K.-H.; Sirringhaus, H.; Friend, R. H. *Nature* **2005**, *434*, 194–199.
 (88) Veres, J.; Ogier, S.; Lloyd, G. *Chem. Mater.* **2004**, *16*, 4543–4555.

Table 4. Device Configurations and Mobilities of Holes μ_h and Electrons μ_e of Devices of P1

type	gate	insulator	contacts	T_a (°C) ^a	μ_h (cm ² V ⁻¹ s ⁻¹)	μ_e (cm ² V ⁻¹ s ⁻¹)
A	Si BG	SiO ₂	Au BC	120	1×10^{-6}	4×10^{-6}
B	Si BG	SiO ₂ /PPcB	Au TC	120	3×10^{-5}	3×10^{-5}

^a T_a = annealing temperature.

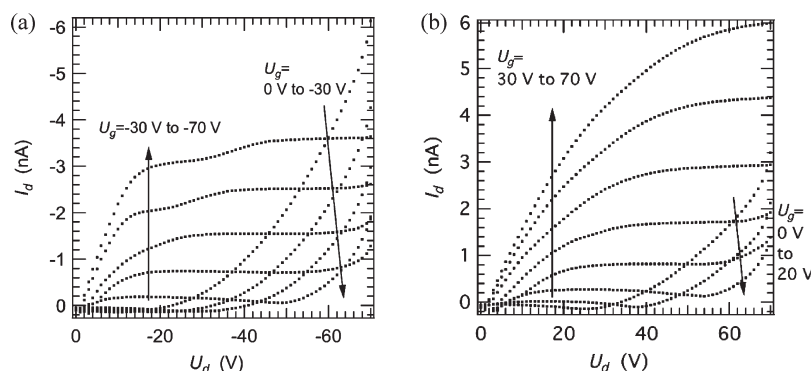


Figure 10. Output characteristics of device B in the (a) hole and (b) electron accumulation mode. U_g is varied from 0 to 70 V in steps of 10 V. Transistor details: $W = 2$ mm, $L = 125$ μ m.

mobilities measured on untreated SiO₂ surfaces. This is possibly caused by the high electron affinity (EA) of P1, because materials of high EA (> 4 eV) were found to be less affected by the presence of electron traps.⁸⁹ The suppression of the hole transport might originate from additional energetic disorder induced at the P1/SiO₂ interface by the polarity of the SiO₂ surface,⁸⁸ which according to the charge transport model for disordered semiconductors proposed by Bäessler,⁹⁰ leads to a broadening of the Gaussian density of states and thus to an enhanced localization of charge carriers.⁹¹

The output characteristics of device B in the hole and electron accumulation mode are displayed in panels a and b in Figure 10, respectively, and the corresponding transfer characteristics are shown in Figure 11.

Nicely balanced ambipolar transport is clearly observed with hole and electron mobilities of 3×10^{-5} cm² V⁻¹ s⁻¹. The contact resistance does not dominate the charge transport as can be seen from the linear onset of the drain current of the output characteristics. This is expected from the HOMO and LUMO levels of P1 estimated to be -5.5 and -4.5 eV, respectively. The threshold voltages for hole and electron accumulation are -19 and 9 V, respectively, and a considerable hysteresis is observed in the ambipolar regime of the transfer characteristics. This hysteresis might arise from trap filling by the accumulated charge carrier species, which enhances the drain current in backward direction. These traps can have their origin in the tail of the intrinsic density of states distribution, or in Coulomb interaction with trapped charges of the opposite sign. Also metallic or organic impurities could limit the charge transport. Another reason for the low mobilities

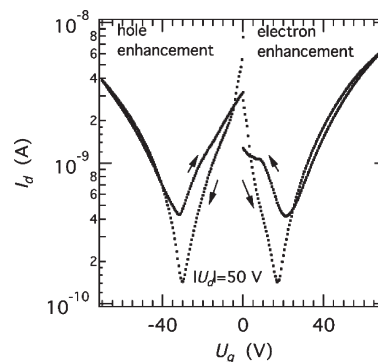


Figure 11. Transfer plot of device B.

could be a nonoptimized morphology. However, annealing altered neither the field-effect transistor characteristics nor the absorption spectra of thin films of P1 (see optical properties), which points to an amorphous material. Since the film morphology of amorphous semiconductors is rather independent of processing procedures and the type of underlying dielectric, as is found for polytriarylamine OFET devices,⁹¹ ordering by a morphology optimization is not expected to be achieved for P1. Note however, that even amorphous semiconductors (polytriarylamines) may exhibit considerably high hole mobilities up to 0.01 cm² V⁻¹ s⁻¹.⁸⁸ Therefore, comparing the polymer structures of high mobility semiconductors to that of P1, the low mobility is presumably caused by the lack of close packing of the polymer chains: In contrast to the flat, planar backbone structures of diketopyrrolopyrrole based polymers^{73,92} P1 has a flexible and twisted backbone structure. The weak intermolecular interactions are also visible by the close similarity of absorption spectra in

(89) Yoon, M.-H.; Kim, C.; Facchetti, A.; Marks, T. J. *J. Am. Chem. Soc.* **2006**, *128*, 12851–12869.

(90) Bäessler, H. *Phys. Status Solidi B* **1993**, *175*, 15–56.

(91) Veres, J.; Ogier, S. D.; Leeming, S. W.; Cupertino, D. C.; Khaffaf, S. M. *Adv. Funct. Mater.* **2003**, *13*, 199–204.

(92) Bijleveld, J. C.; Zoombelt, A. P.; Mathijssen, S. G. J.; Wienk, M. M.; Turbiez, M.; de Leeuw, D. M.; Janssen, R. A. J. *J. Am. Chem. Soc.* **2009**, *131*, 16616–16617.

solution and in the film which implies the absence of excitonic interactions in the solid state.

Conclusions

Polyradical **P1** is the first polymeric neutral MV compound which was synthesized by Horner-Emmons reaction. Comparison with the monomer analogue **M** shows that the lowest-energy band of **P1** can be interpreted as an IV-CT transition that is associated with an optically induced transfer of an electron from the donor (triarylamine) to the radical acceptor (PCTM) unit. The electronic coupling between donor and acceptor states has the same magnitude as in the monomer, that is ca. 2000 cm^{-1} . Despite the connection of repeating units by conjugated bridges the IV-CT transition of **P1** is confined to one donor/acceptor pair which is proved by the close similarity of polymer and monomer electronic spectra. However, for the more intense, higher energy transitions a distinct excitonic broadening of bands is observed. The band gap of the polymer was determined by both optical (1.2 eV) and electrochemical methods (1.0 eV). The somewhat lower electrochemical band gap compared to the optical band gap may be primarily explained by ion pairing effects and indicates a very low exciton binding energy. The major difference between monomer and polymer is the good film-forming property of **P1** which forms amorphous films that are stable upon annealing at $110\text{ }^{\circ}\text{C}$ in air.

The ET properties of **P1** were investigated in solution by fs-pump-probe transient absorption spectroscopy whereas the charge transport characteristics were investigated in films in two different OFET configurations.

(93) One referee suggested an alternative explanation for τ_3 according to which the formation of CS states is driven by excess energy of the initial excitation. The charge recombination is then exergonic and unidirectional provided that there is a sizable exciton binding energy. Although the inaccuracy of the rate constants, and thus the equilibrium constants, would allow such an interpretation, we are currently unable to provide evidence for this mechanism by, for example, lowering the excitation energy due to experimental limitations of our laser setup.

The optical pump-probe experiments revealed distinct differences between monomer and polymer. The transient spectra of both systems unequivocally prove a charge separation in the IV-CT state as evidenced by the results of spectroelectrochemical measurements. Although the monomer shows a single decay time which strongly depends on the solvent polarity, the polymer has a biexponential decay with an additional-solvent independent-slow decay component. The short-living component is interpreted as the direct decay from the IV-CT state to the ground state and the long-living component as an equilibrium formation of the IV-CT state and a completely charge-separated state. This hypothesis is supported by the observation of a small exciton binding energy as well as by the excited state equilibrium constants of ca. 0.5 and 1.4 in toluene and dichloromethane, respectively.

Charge-carrier mobilities were measured in two different OFET configurations both for electron and for hole migration. Using an insulating organic PPcB layer increases the mobilities by 1 order of magnitude to ca. $3 \times 10^{-5}\text{ cm}^2\text{ V}^{-1}\text{ s}^{-1}$ for both charge carriers. While the **P1** films show a well-balanced ambipolar transport promoted by the small injection barriers into HOMO (-5.5 eV) and LUMO (-4.5 eV) level, respectively, the overall mobilities are relatively low probably because of less densely packed polymer chains caused by the propeller-like PCTM and triarylamine moieties.

In conclusion, although the spin aspects of polyradical **P1** have been neglected in the present study the promising ET and charge-transport properties open the chance to use **P1** in photonic/electronic and, possibly, spintronic devices.

Acknowledgment. We thank Sabine Keiber, Johannes Buback, Patrick Nürnberger, Daniel Rauh, Julian Friedrich, Alexander Heckmann, Alexander Schmiedel, Matthias Stolte and Vladimir Stepanenko for their interest and experimental support and the Deutsche Forschungsgemeinschaft for financial support (GRK 1221 and La 991/12).